Inorganic Chemistry

Article

pubs.acs.org/IC

Design of Single-Molecule Magnets: Insufficiency of the Anisotropy Barrier as the Sole Criterion

Kasper S. Pedersen,*[†,‡,§] Jan Dreiser,[∥,⊥] Høgni Weihe,[†] Romain Sibille,[@] Heini V. Johannesen,[†] Mikkel A. Sørensen,[†] Bjarne E. Nielsen,[†] Marc Sigrist,[†,#] Hannu Mutka,[#] Stephane Rols,[#] Jesper Bendix,*[†] and Stergios Piligkos*[†]

[†]Department of Chemistry, University of Copenhagen, Universitetsparken 5, DK-2100 Copenhagen, Denmark

[‡]CNRS, CRPP, UPR 8641, F-33600 Pessac, France

[§]CNRS, ICMCB, UPR 9014, F-33600 Pessac, France

[∥]Institute of Condensed Matter Physics, Ecole Polytechnique Fédérale de Lausanne, CH-1015 Lausanne, Switzerland

[⊥]Swiss Light Source, Paul Scherrer Institut, CH-5232 Villigen PSI, Switzerland

[@]Laboratory for Developments and Methods, Paul Scherrer Institut, CH-5232 Villigen PSI, Switzerland

[#]Institut Laue-Langevin, Grenoble, France

Supporting Information

ABSTRACT: Determination of the electronic energy spectrum of a trigonal-symmetry mononuclear Yb^{3+} single-molecule magnet (SMM) by high-resolution absorption and luminescence spectroscopies reveals that the first excited electronic doublet is placed nearly 500 cm^{-1} above the ground one. Fitting of the paramagnetic relaxation times of this SMM to a thermally activated (Orbach) model $\{\tau = \tau_0 \times \exp[\Delta_{\mathrm{Orbach}}/(k_B T)]\}$ affords an activation barrier, Δ_{Orbach}, of only 38 cm^{-1}. This result is incompatible with the spectroscopic observations. Thus, we unambiguously demonstrate, solely on the basis of experimental data, that Orbach relaxation cannot *a priori* be considered as the main mechanism determining the spin dynamics of SMMs. This study highlights the fact that the general synthetic approach of optimizing SMM behavior by maximization of the anisotropy barrier, intimately linked to the ligand field, as the sole parameter to be tuned, is insufficient because of the complete neglect of the interaction of the magnetic moment of the molecule with its environment. The Orbach mechanism is expected dominant only in the cases in which the energy of the excited ligand field state is below the Debye temperature, which is typically low for molecular crystals and, thus, prevents the use of the anisotropy barrier as a design criterion for the realization of high-temperature SMMs. Therefore, consideration of additional design criteria that address the presence of alternative relaxation processes beyond the traditional double-well picture is required.

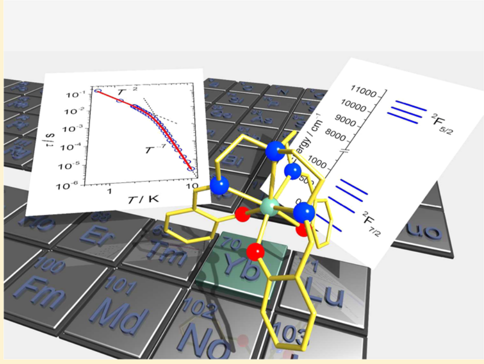

■ INTRODUCTION

Single-molecule magnets (SMMs) are paramagnetic metal complexes exhibiting magnetization bistability in the absence of long-range magnetic order.[1] Mononuclear SMMs, i.e., SMMs encompassing only a single paramagnetic center, have been proposed as candidates for spin valves, quantum computing, and data storage applications where lanthanides, in particular, provide the strong magnetic anisotropy necessary for such realizations.[2,3] Lanthanide-based systems have, in just a few years, surpassed even the best-performing transition metal-based systems with reported record-large coercive fields and spin-reversal energy barriers approaching 1000 K.[4−6] Any applications of the memory effect of lanthanide-based SMMs fundamentally rely on the maximization of this barrier that provides for high-temperature magnetic hysteresis. For lanthanide ions, the fine structure, which is the relative energies of sublevels within a spectroscopic term, is very sensitive to the ligand field experienced by the lanthanide center. Therefore, modeling of the magnetic properties of lanthanide-based SMMs is most often kept at a qualitative level, because any quantitative approach requires the determination of a large number of ligand field parameters, as many as 27 for low-symmetry complexes. These ligand field parameters can, in principle, be determined by use of spectroscopic methods such as absorption and luminescence spectroscopies, but in practice, spectral broadening and low molecular symmetry make the determination of such a large number of ligand field parameters impossible. To alleviate this situation, quantum computational approaches can provide insight into the electronic structure of such lanthanide-based SMMs.[7] However, because high-level computations are required, such computational approaches

Received: May 28, 2015
Published: July 22, 2015

ACS Publications

DOI: 10.1021/acs.inorgchem.5b01209
Inorg. Chem. 2015, 54, 7600−7606

remain quite challenging and still generally require support from experimental data.[8] In theoretical and spectroscopic studies of the electronic energy spectrum of lanthanide-based SMMs, comparisons are normally made between the calculated, or the spectroscopic, energy splitting between the ground and first excited ligand field state with the experimentally derived energy barrier for spin reversal. In the vast majority of reported studies, such spin-reversal barriers are extracted from temperature- and frequency-dependent alternating current (ac) magnetic susceptibility measurements, by modeling the data assuming only a thermally activated Orbach process.[9,10] This Orbach process, for which the relaxation time, τ, is given by $\tau = \tau_0 \times \exp[\Delta_{\mathrm{Orbach}}/(k_B T)]$, where Δ_{Orbach} designates an "energy barrier" via an excited ligand (crystal) field state,[9,11] results in a linear dependence in the Arrhenius plot, i.e., of $\ln(\tau)$ versus T^{-1}, with T being the temperature. In some studies, the energy of the first excited state has been determined by inelastic neutron scattering (INS),[12,13] frequency-domain EPR,[13] or luminescence spectroscopy,[14] leading, in some cases, to good agreement with the extracted Δ_{Orbach}.[2a] However, in most of these studies, large discrepancies are observed between the linearity expected from an Orbach mechanism and the experimental data.[15] This has often been ascribed to the occurrence of temperature-independent quantum tunnelling of the magnetization (QTM).[10,16] Δ_{Orbach} is usually not determined directly by spectroscopic methods because the associated electronic transitions are not always possible to observe and, when observed, are often difficult to discriminate from vibrational modes, including lattice phonons.

Herein, we present a study of the crystallographically trigonal ytterbium(III) SMM: Yb(trensal) [**1** (Figure 1)], where H$_3$trensal is 2,2′,2″-tris(salicylideneimino)triethylamine.[17] The system is part of an isostructural series of lanthanide complexes for which the ligand field parameters (except for Yb^{3+}) were reported by Riley and co-workers,[18] and the magnetic properties of the Tb^{3+}, Dy^{3+}, and Er^{3+} analogues studied by Sorace, Dreiser, Sessoli, and their co-workers.[12,19,20] The trigonal symmetry of **1** ($P\bar{3}c1$ space group) results in a drastic reduction in the ligand field parameters necessary for the description of its electronic energy spectrum. For trigonal symmetry, only eight independent ligand field parameters are necessary for this purpose. The precise determination of the electronic energy spectrum of **1**, obtained by high-resolution absorption and luminescence spectroscopies, in conjunction with electron paramagnetic resonance (EPR) spectroscopy and detailed single-crystal magnetization measurements, provides a rare possibility of an in-depth analysis of the processes governing the magnetization dynamics of a mononuclear SMM. This analysis results in the unambiguous assertion that the Orbach relaxation process is not governing the spin dynamics of **1**. Thus, simply maximizing the energy barrier of SMMs is not enough to realize enhanced dynamic magnetic properties. Additional design criteria that consider the vibrational modes of the studied system have to be taken into account for this purpose.

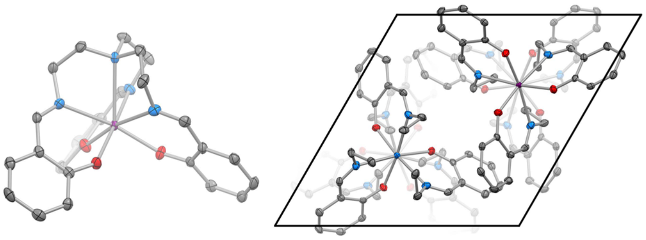

Figure 1. X-ray crystal structure of **1** at 122(1) K (thermal ellipsoids drawn at the 70% probability level). Color code: purple, ytterbium; red, oxygen; blue, nitrogen; gray, carbon. Hydrogen atoms have been omitted for the sake of clarity. The unit cell content ($Z = 4$) along the crystallographic c axis is shown at the right.

RESULTS AND DISCUSSION

Single-crystal and polycrystalline powder, direct current (dc) magnetization data of **1** are shown in Figure 2. Notably, the χT product (2.0 cm^3 K mol^{-1}) of polycrystalline **1** at 280 K is much lower than the Curie constant of Yb^{3+} (2.57 cm^3 K mol^{-1}, for $^2F_{7/2}$, $g_J = 8/7$), suggesting that the energy separation between the ground and the highest excited Kramers doublet of the $J = 7/2$ ground term is on the order of magnitude of the thermal energy at this temperature, or larger. Given the trigonal crystallographic symmetry of **1**, magnetization measurements only parallel ($\boldsymbol{H}\|C_3$) and perpendicular ($\boldsymbol{H}\perp C_3$) to the crystallographic c axis are needed to determine the susceptibility tensor. Such measurements show that **1** is an "easy-axis" system, with $M_{H\|C_3} > M_{H\perp C_3}$ (Figure 2).

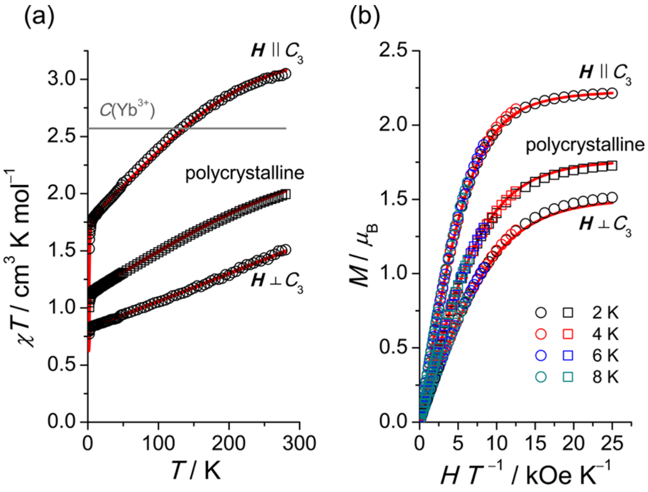

Figure 2. Static (dc) magnetization data of a single crystal and a polycrystalline sample of **1**. (a) $\chi T(T)$ obtained with $H_{\mathrm{dc}} = 10$ kOe. (b) Low-temperature magnetization vs HT^{-1}. The solid lines are best fits as described in the text. Only the $T = 2$ K fit is shown in the right panel.

Single-crystal X-band EPR spectra of isostructural Eu(trensal) doped with ~5% Yb^{3+} are shown in Figure 3. The spectra consist of resolved resonances originating from Yb^{3+} species with or without a nuclear spin. Analysis of these EPR spectra, treating the Yb^{3+} as an effective spin-$^1/_2$ ion, allows determination of the relevant g factors ($g_\| = 4.29$, and $g_\perp = 2.90$) and hyperfine coupling constants [$A_\|^{I=5/2} = -0.03123(1)$ cm^{-1}, $A_\perp^{I=5/2} = -0.02244(9)$ cm^{-1}, $A_\|^{I=1/2} = 0.11243(4)$ cm^{-1}, and $A_\perp^{I=1/2} = 0.07407(4)$ cm^{-1}].

The precise determination of the electronic energy spectrum of **1** is only possible by a simultaneous analysis of its high-resolution absorption and luminescence spectra, rendering feasible the assignment of the electronic or vibrational nature of the observed bands. The temperature-dependent $^2F_{7/2} \rightarrow {}^2F_{5/2}$ absorption spectra of **1** (Figure 4, bottom) feature three prominent bands at 11074 cm^{-1} (c1), 10661 cm^{-1} (c2), and

DOI: 10.1021/acs.inorgchem.5b01209
Inorg. Chem. 2015, 54, 7600−7606

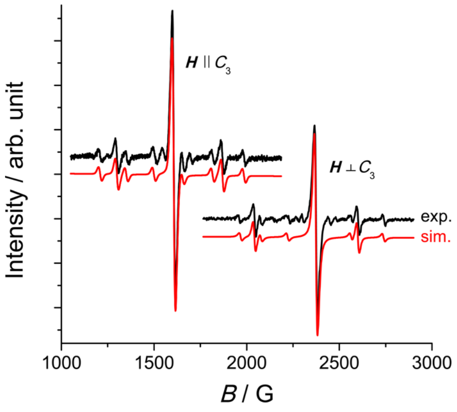

Figure 3. Single-crystal X-band (f = 9.62 GHz) EPR spectra obtained at T = 10 K of ~5% Yb^{3+} in Eu(trensal). The red lines are simulations using the g factors and the hyperfine coupling parameters given in the text and natural abundances of ^{171}Yb ($I = {}^{1}/_{2}$) and ^{173}Yb ($I = {}^{5}/_{2}$) of 14 and 16%, respectively.

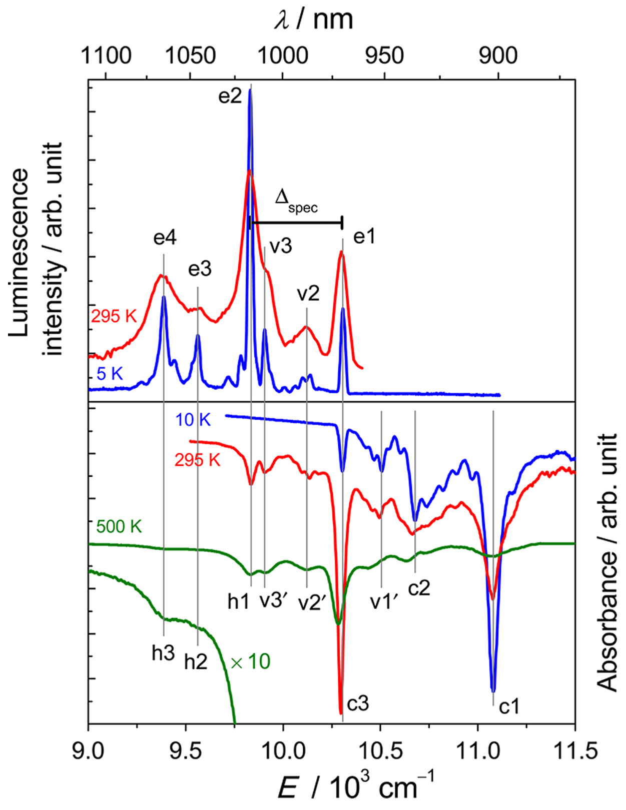

Figure 4. NIR data of **1** (single-crystal absorption, $^2F_{7/2} \rightarrow {}^2F_{5/2}$) and **1′** (powder, luminescence, $^2F_{7/2} \leftarrow {}^2F_{5/2}$). c, h, e, and v denote cold absorption, hot absorption, emission, and vibrational transitions, respectively. A magnification of the 500 K absorption spectrum is shown to highlight h2 and h3. Vertical lines are guides for the eye.

10299 cm^{-1} (c3). Four additional bands are clearly observed at 10504 cm^{-1} (v1′), 10125 cm^{-1} (v2′), 9903 cm^{-1} (v3′), and 9835 cm^{-1} (h1), of which v3′ and h1 are observed only at the highest temperatures.

By taking advantage of the characteristic $^2F_{7/2} \leftarrow {}^2F_{5/2}$ near-infrared (NIR) luminescence of Yb^{3+}, we can acquire fundamental information about the splitting of the $^2F_{7/2}$ multiplet due to the ligand field. Temperature-dependent luminescence spectra of ~10% Yb^{3+} doped into Y(trensal) polycrystalline powder (**1′**) acquired by excitation in a ligand absorption band (λ_{ex} = 360 nm; E_{ex} = 27778 cm^{-1}) are shown in the top panel of Figure 4. Five prominent bands are discernible at energies of 10299 cm^{-1} (e1), 9903 cm^{-1} (v3), 9835 cm^{-1} (e2), 9563 cm^{-1} (e3), and 9387 cm^{-1} (e4). The highest-energy emission peak (e1) coincides in energy with the lowest-energy excitation (c3) of the 10 K absorption spectrum and is thus assigned as the "zero-phonon" line. Excitation in an f−f absorption band for the concentrated sample of **1** gave essentially identical spectra (cf. Figure S1 of the Supporting Information), the only difference being the absence of e1, which is attributed to re-absorption through the c3 excitation. Given that band c3 is the lowest-energy excitation originating from the ground Kramers doublet of the $^2F_{7/2}$ term, we assign bands c2 and c1 to excitations from the same doublet to the two remaining excited doublets of $^2F_{5/2}$. Bands v3 and e2 coincide with bands v3′ and h1 in the high-temperature absorption spectra. The experiments cannot unambiguously discriminate between the nature of e2 and v3. Here we assume e2 as an emission from the ground doublet of the excited $^2F_{5/2}$ term to the first excited doublet of the ground $^2F_{7/2}$ term. This is corroborated by the qualitative resemblance of the energy level diagram of **1** calculated on the basis of published ligand field parameters for the isostructural Er^{3+} and Tm^{3+} systems (cf. Figure S4 of the Supporting Information).[18] Hence, h1 can be identified as the reverse process. In addition, this agrees with the common practice of assigning the most intense emission bands as being of electronic origin. Similarly, bands e3 and e4 are assigned as the remaining emissions from the ground doublet of $^2F_{5/2}$ to $^2F_{7/2}$. The reverse processes are assigned to bands h2 and h3, respectively, observed only in the 500 K spectrum. It should be noted here that the thermal stability of the isostructural Er(trensal) has been demonstrated up to at least 557 K.[21]

In this picture, the energy difference between h1 and c3 and between e1 and e2, hereafter termed Δ_{spec}, directly measures the energy separation between the ground and first excited Kramers doublets of $^2F_{7/2}$. Thus, Δ_{spec} amounts to 464 cm^{-1}. On the basis of this splitting, the calculated ratio of the intensity of h1 at 295 and 100 K is approximately 1%, in good agreement with experiment (cf. Figure S3 of the Supporting Information). The extracted energy level diagram is shown in Figure 5.

From the aforementioned calculations assuming direct transferability of the Er(trensal) and Tm(trensal) ligand field parameters,[18] Δ_{spec} is calculated to be 552 and 512 cm^{-1}, respectively, in reasonable agreement with experiment (cf. Figure S4 of the Supporting Information). Because of the large splittings in the $^2F_{5/2}$ multiplet, as evidenced by the energy difference of bands c1−c3, emissions from excited states of $^2F_{5/2}$ are unlikely at low temperatures.[22] Thus, the vibrational structure of the 5 K luminescence spectrum originates from vibronic levels of the ground $^2F_{7/2}$ multiplet. The shape of band v2 and its energy separation from band e1 (170 cm^{-1}) indicate that v2 is part of the vibrational sideband of e1.[22] On the other hand, v1′ is assigned as the vibrational structure of the ground doublet of $^2F_{5/2}$, which is corroborated by the nearly symmetrical placement of v2 and v1′ around e1 or c3. Band v2′ is assigned to the reverse process of band v2. This plethora of vibrational sidebands appears to always be present in Yb^{3+} systems, and in the literature, it is thought to be an intrinsic property of the electronic structure of Yb^{3+}.[23] Attempts to observe magnetic excitations by INS spectroscopy on **1** were unsuccessful (Figures S7 and S8 of the Supporting

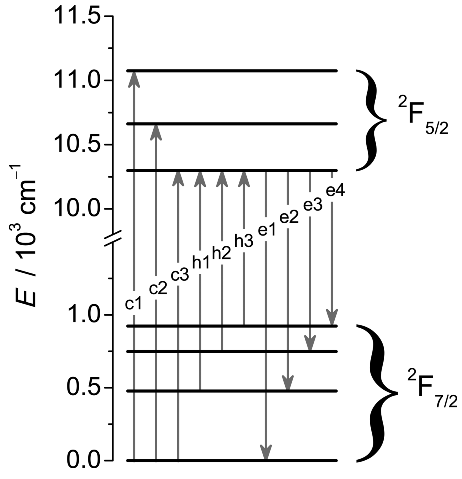

Figure 5. Energy level diagram of **1** as extracted from the analysis of luminescence and absorption spectra. Each horizontal line represents a Kramers doublet, and c, h, and e denote cold absorption, hot absorption and emission, respectively.

Information), likely a result of the overall weakness of the expected magnetic contribution, because of the small magnetic moment and the presence of strong nuclear inelastic contributions. To the best of our knowledge, only one Yb^{3+} complex has been studied by INS spectroscopy, namely $(PPh_4)_2[Yb(NO_3)_5]$, but in this case, the first excited state was placed only 16 cm^{-1} over the ground state doublet, which facilitated the observation of an INS transition.[24] In fact, for **1**, the ratios of the scattering cross section originating from ^1H and Yb^{3+} to the total scattering cross section are $\sigma_H/\sigma_S \approx 0.91$ and $\sigma_{Yb}/\sigma_S \approx 0.009$, respectively, meaning that the inelastic spectrum, in certain regions, is completely dominated by ^1H vibrations.

To determine the ligand field parameters of **1**, we adopt an approach similar to that adopted by Riley and co-workers.[18] To describe the electronic energy spectrum of **1**, we use a ligand field Hamiltonian that takes into account the spin−orbit coupling constant of Yb^{3+}, ζ_{SO}, and all symmetry-allowed parameters, namely, B_{20}, B_{40}, Re(B_{43}), Im(B_{43}), B_{60}, Re(B_{63}), Im(B_{63}), Re(B_{66}), and Im(B_{66}), associated with operators acting on f-orbitals. Taking into account the six independent energy splittings derived from optical spectroscopy, as well as the two orientation-dependent EPR observations, we fit the ligand field Hamiltonian to these experimental observables. For this purpose, we set Im(B_{43}) and B_{40} equal to zero. Setting Im(B_{43}) to zero corresponds to fixing the x-axis direction in the C_3 point group. Setting B_{40} equal to zero is justified by the fact that the magnitude of the B_{40} ligand field parameter was found to vary almost randomly around zero across the Ln(trensal) series, with associated error bars of the same order of magnitude, or larger, as the parameter value.[18] The resulting ligand field parameters (Table S2 of the Supporting Information) are in very good agreement with those presented by Riley for the rest of the Ln(trensal) series.[18] This transferability of f-orbital ligand field parameters across the Ln(trensal) series is also illustrated by the fact that computation of the electronic spectrum of **1** using the ligand field parameters pertinent to Tm(trensal) results in an energy level diagram agreeing very well with the experimentally determined energy spectrum of **1** (Figure S4 of the Supporting Information).

The spectroscopic data together with the static magnetic data were modeled by use of the Hamiltonian (eq 1) pertinent to the ground state multiplet of **1**:

$$\hat{H} = \sum_{k,-k\leq q\leq k} B_k^q \hat{O}_k^q + g_J\mu_B\mu_0\hat{\mathbf{J}}\cdot\mathbf{H} \qquad (1)$$

where B_k^q is a Stevens operator coefficient (parameter), $g_J = {}^8/_7$ is the Landé g factor, and $J = {}^7/_2$ is the total angular momentum corresponding to the $^2F_{7/2}$ ground state of the Yb^{3+} ion. Notice that the notation used to describe the Stevens operator coefficients differs from the one used above to describe the f-orbital ligand field parameters in the use of both super- and subscripts for the former. The Hamiltonian (eq 1) was simultaneously fitted to (a) the χT product of **1** measured with the magnetic field parallel and perpendicular to the C_3 axis

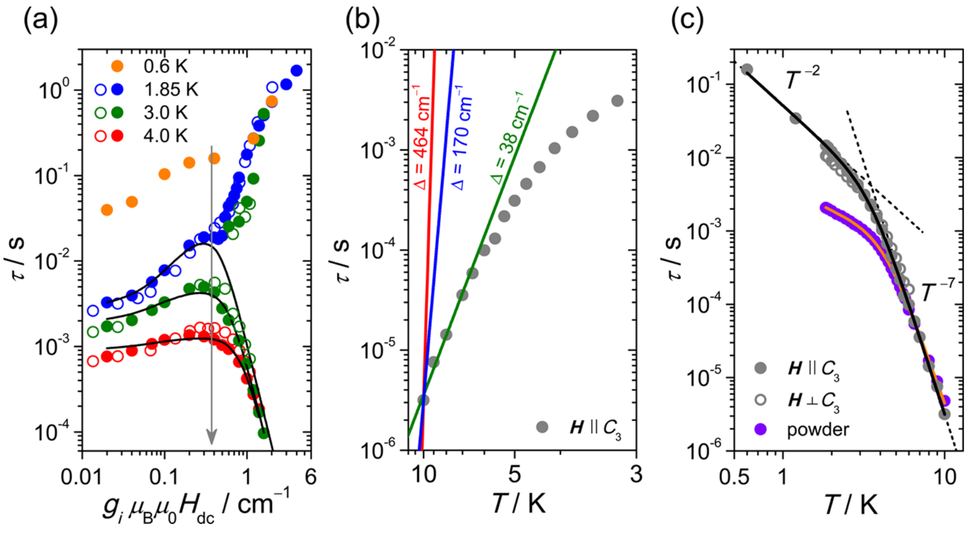

Figure 6. (a) Field and orientation dependence of the relaxation time at selected temperatures presented in a double-logarithmic plot: (●) $\boldsymbol{H}\|C_3$ and (○) $\boldsymbol{H}\perp C_3$. For 3 K, the occurrence of both an upturn and downturn results from two distinct relaxation regimes. Solid lines were calculated as described in the text. The arrow indicates H_{dc} = 2000 Oe for $\boldsymbol{H}\|C_3$. (b) Arrhenius plot (reciprocal temperature axis) showing the temperature dependence of the relaxation time at H_{dc} = 2000 Oe for **1** ($\boldsymbol{H}\|C_3$) together with the calculated slopes for Orbach processes as discussed in the text. (c) Double-logarithmic plot of the temperature dependence of the relaxation time at H_{dc} = 2000 Oe for **1** and fits as described in the text.

DOI: 10.1021/acs.inorgchem.5b01209
Inorg. Chem. 2015, 54, 7600−7606

on a single crystal of **1**, (b) the field-dependent magnetization $M(H)$ of a single crystal of **1** at 2 K, for the same orientations of the magnetic field as in part a, and (c) the energy differences of the sublevels of the $^2F_{7/2}$ ground state multiplet determined via optical spectroscopy. Upon variation of all symmetry-allowed Stevens parameters (fit 0 in Table S3 of the Supporting Information), excellent agreement with the experimental data is achieved (Figure 2 and Table S3 of the Supporting Information). Fixing B_4^{-3} to zero results in four physically equivalent parameter sets (fits 1–4 in Table S3 of the Supporting Information).

Having firmly established the energy spectrum of **1**, we turn our attention to the dynamical properties of the system. The easy axis-type magnetization is considered a common prerequisite for obtaining SMM properties, although notable exceptions have been reported.[19,25] Single-crystal and powder ac susceptibility data of **1** are shown in Figures S9–S16 and S18–S20 of the Supporting Information. To the best of our knowledge, only one study has reported the orientational dependence of the ac susceptibility of an SMM.[26] Therein, however, the strong anisotropy prevented the observation of any frequency dependence when the ac field was applied perpendicular to the easy axis of magnetization.

For **1**, in the absence of a static dc field, no out-of-phase component, χ'', was observed for any of the orientations ($\boldsymbol{h}_{ac}||C_3$ and $\boldsymbol{h}_{ac}\perp C_3$). Application of just a small static field gives rise to clear χ'' maxima for both orientations, and for fields from ~1.5 kOe and up, χ' approaches zero at the highest frequencies (1.5 kHz), indicative of full blocking of the magnetization.[27] The relaxation times, τ, were extracted from fits to a generalized Debye model[28] and are shown in Figure 6a. These relaxation times are distinctly anisotropic with respect to the orientation of the applied static magnetic field. In Figure 6a, the extracted relaxation times are plotted with the abscissa scaled to the Zeeman energy difference of the two components of the ground Kramers doublet, along each of the two orientations ($\boldsymbol{H}||C_3$ and $\boldsymbol{H}\perp C_3$). For this purpose, we use the effective g factors of the respective orientations: $g_{||} = 4.4$ and $g_{\perp} = 3.0$ (Figure S6 of the Supporting Information) when treating the Yb^{3+} as an effective spin-half system. Thus, τ is presented with respect to the Zeeman splitting of the ground Kramers doublet. In this representation, the relaxation times for the two orientations become nearly superimposable. This applies throughout the studied static field range, where the extracted relaxation times exhibit quite complicated field dependencies (Figure 6a). Thus, the multiple mechanisms required to yield the observed, complex dependence of τ on the static field strength can all be seen to depend in a similar way on the splitting of the ground state Kramers doublet. Given the intercomplex separations of 7.6 Å, the maximal dipolar energy can be estimated as $\mu_0\mu_B{}^2g_{||}{}^2(1/2)^2/(4\pi r_{Yb-Yb})^3 \approx 5 \times 10^{-3}$ cm^{-1} and is thus expected to be of minor importance for the relaxation dynamics. Notably, at the lowest temperatures, τ increases steadily with H until reaching a plateau at ~0.4 cm^{-1} (corresponding to 2000 Oe for $\boldsymbol{H}||C_3$), after which an abrupt increase occurs. While the former increase can be attributed to the slowing of the relaxation due to the quenching of tunnelling pathways, the latter is suggestive of phonon-bottleneck effects.[29] This is further supported by the dramatic increase in the distribution parameter, α, of the generalized Debye function when approaching a Zeeman energy of ~1 cm^{-1} (cf. Figure S17 of the Supporting Information). The χ' and χ'' data at 0.6 and 1.85 K can be modeled by the inclusion of only one relaxation process, while the higher-temperature data suggest the existence of two coexisting, distinct processes (cf. Figures S12–S16 of the Supporting Information). For 3 and 4 K, τ experiences a fast decrease at higher fields, as expected for a direct process becoming more important (Figure 6a).[9] When QTM (B_1 and B_2 parameters), the direct process (A parameter), and a field-independent relaxation process (k parameter) are taken into account, τ can be modeled by the expression[12,19,30]

$$\tau^{-1} = \frac{B_1}{1 + B_2H^2} + ATH^4 + k(T) \tag{2}$$

The solid lines of Figure 6a are calculated for $\boldsymbol{H}||C_3$ with $B_1 = 3 \times 10^2$ s^{-1}, $B_2 = 9 \times 10^{-6}$ Oe^{2-}, $A = 8 \times 10^{-13}$ s^{-1} K^{-1} Oe^{4-}, and $k(T)$ = 30, 200, and 800 s^{-1} for 1.85, 3, and 4 K, respectively. Compensation of the hyperfine interaction energy (A_iIS) by the Zeeman energy ($g_i\mu_B\mu_0HS$) is achieved at approximately the same applied magnetic fields, even though $g_{||} > g_{\perp}$, as $A_{||}{}^{I=1/2}/g_{||} \approx A_{\perp}{}^{I=1/2}/g_{\perp}$ and $A_{||}{}^{I=5/2}/g_{||} \approx A_{\perp}{}^{I=5/2}/g_{\perp}$. Thus, the "hyperfine" field, H_{hyp}, is independent of the orientation through $H_{hyp} = (A_i/g_i) \times I/(\mu_B\mu_0)$. Furthermore, the remaining 70% of Yb^{3+} not bearing a nuclear spin does not appear to possess spin relaxation dynamics different from those of the isotopes bearing a nuclear spin, as evidenced by the absence of discernible relaxation regimes in the low-field dynamic susceptibility measurements (Figures S9–S16 of the Supporting Information).

The temperature dependence of τ was studied at a field of 2000 Oe (arrow in Figure 6a) for both $\boldsymbol{H}||C_3$ and $\boldsymbol{H}\perp C_3$ and for a polycrystalline powder (Figures S18–S20 of the Supporting Information). The extracted relaxation times for $\boldsymbol{H}||C_3$ data are presented as an Arrhenius plot in Figure 6b. In addition, the extracted relaxation times for $\boldsymbol{H}||C_3$ and $\boldsymbol{H}\perp C_3$ and for a polycrystalline powder are shown in the double-logarithmic plot of Figure 6c. Notably, no clear linear region of the former is observed. Fitting of τ to an Orbach model of the form $\tau = \tau_0 \times \exp[\Delta_{Orbach}/(k_BT)]$ yields Δ_{Orbach} = 38 cm^{-1} and $\tau_0 = 1.5 \times 10^{-8}$ s. The low-temperature extrapolated fit for these parameters is shown in Figure 6b as a solid green line (inset). Following Orbach's theory, this mechanism requires excitation to an excited ligand (crystal) field state by interaction with the thermal bath.[9,11] However, as is evident from the preceding analysis of the absorption and luminescence spectra, the energy of the first excited Kramers doublet of **1** is at Δ_{spec} = 464 cm^{-1}.[31] The simulated behavior for Δ_{Orbach} = 464 cm^{-1} is shown in Figure 6b as a solid red line. Thus, analysis of the experimental spectroscopic and magnetization data shows that the relaxation dynamics of **1**, expected from an assumed Orbach relaxation process, is in strong contrast with the observed nonlinearity of ln(τ) versus T^{-1}. Furthermore, the energy barrier, Δ_{Orbach}, associated with this assumed Orbach relaxation process is one order of magnitude smaller than the smallest observed, by spectroscopic methods, energy splitting, Δ_{spec}, in **1**. These observations unambiguously demonstrate the irrelevance of the Orbach relaxation mechanism with respect to the spin dynamics of **1**, at these temperatures. While a few studies have previously indicated a discrepancy between Δ_{spec} and Δ_{Orbach}, the mismatch has been far less dramatic than in the case presented here. For instance, in Er(trensal), Δ_{Orbach} was estimated to be 20 cm^{-1},[12] or 22 cm^{-1},[19] while Δ_{spec} was determined to be 54 or 52 cm^{-1} by luminescence or INS spectroscopy, respectively.[32,12]

On the contrary, for $\boldsymbol{H}||C_3$, in the double-logarithmic plot of Figure 6c, τ exhibits a large degree of linearity of the high- and low-temperature regions suggesting a power law description of $\tau \propto T^{-n}$ (Figure 6c). Such behavior is reminiscent of the alternative Raman relaxation mechanism, which is manifested by its strong temperature dependence following a power law with typical exponents, n, between 5 and 9.[33] Fitting of the complete temperature-range data of $\boldsymbol{H}||C_3$ to a sum of two power laws dominating at high and low temperature, respectively

$$\tau^{-1} = CT^n + DT^m \tag{3}$$

affords $C = 0.044$ s^{-1} K$^{-6.9}$, $n = 6.9$ (high temperature), and $D = 19$ s^{-1} K^{-2} (low temperature). Here, m was fixed to 2 as expected for a phonon-bottleneck-limited direct process.[34] For polycrystalline powder of **1**, the resulting parameters were $C = 0.15$ s^{-1} K$^{-6.2}$, $n = 6.2$, and $D = 258$ s^{-1} K^{-1} with m fixed to 1 as expected for a normal direct process.[9] Note that phonon-bottleneck-limited direct processes are more commonly observed for crystalline samples than for powders (cf. Figure S22 of the Supporting Information).[29] We did not include a temperature-independent QTM term in the fitting of the temperature dependence that may seem surprising given the importance of QTM for the field dependence of τ. The Raman process is expected to be field-dependent only when the applied magnetic field is small as compared to the fields resulting from hyperfine and dipolar interactions. A simple expression was derived by van Vleck[35] but is, according to Orbach,[36] inapplicable for cases in which $g_\perp \neq 0$. Application of the more complicated model unavoidably leads to a vast over-parametrization of the experimental data. Thus, we chose to use the simpler QTM model while keeping in mind the fact that any field dependence of the Raman process may be hidden in the low-field data of Figure 6a.

■ CONCLUSIONS

Our results indicate that in the case of **1**, and in the investigated temperature and field ranges, the relaxation of the magnetization is governed by Raman, direct, and QTM processes. According to our experimental observations, the Orbach relaxation mechanism is not important for the description of the magnetization dynamics of **1**. In addition, a phonon-bottleneck effect was observed for single crystals of **1**. Additionally, the field dependence of the relaxation times is quite complex and anisotropic but becomes identical for the parallel and perpendicular directions to the 3-fold axis when the applied field is scaled with the g values of the ground doublet in the two directions. As demonstrated here, precise determination of the energy spectrum of the studied system is of paramount importance for the understanding of the mechanisms governing its magnetization dynamics. This study demonstrates that the general synthetic approach of optimizing SMM behavior by maximization of the magnetic anisotropy/ligand field-associated energy barrier, as the only synthetic parameter to be tuned, is insufficient because it neglects the interaction of the molecular magnetization with its environment. Indeed, the Orbach mechanism is expected to be dominant only in cases in which the energy of the excited ligand field state is below the Debye temperature, the temperature reflecting the maximal energy of the (acoustic) lattice phonons.[9] Accordingly, the typically low Debye temperature (e.g., $\Theta_D \approx 40$ K for Mn$_{12}$ac)[37] of molecular crystals is likely to impact SMM performance. Therefore, synthetic procedures need to consider additional design criteria that address the presence of alternative relaxation processes besides the Orbach one. Along these lines, optimization of Raman processes by tailoring of lattice phonons appears to be an interesting approach for both yielding further insights and optimizing SMM behavior.

■ ASSOCIATED CONTENT

Ⓢ Supporting Information

Experimental details, additional spectra, and magnetization data. The Supporting Information is available free of charge on the ACS Publications website at DOI: 10.1021/acs.inorgchem.5b01209.

■ AUTHOR INFORMATION

Corresponding Authors

*E-mail: pedersen@crpp-bordeaux.cnrs.fr.
*E-mail: bendix@kiku.dk.
*E-mail: piligkos@kiku.dk.

Notes

The authors declare no competing financial interest.

■ ACKNOWLEDGMENTS

K.S.P. and S.P. thank The Danish Research Council for a DFF Sapere Aude: Research Talent grant (4090-00201) and a Sapere Aude DFF-Starting Grant (10-081659), respectively. Some of the measurements were taken on the PPMS and MPMS devices of the Laboratory for Developments and Methods, Paul Scherrer Institute, Villigen, Switzerland. J.D. gratefully acknowledges funding from the Swiss National Science Foundation (Grant PZ00P2_142474). J.B. acknowledges support from The Danish Research Council under grant 12-125226.

■ REFERENCES

(1) (a) Gatteschi, D.; Sessoli, R.; Villain, J. *Molecular nanomagnets*; Oxford University Press: Oxford, U.K., 2006. (b) Winpenny, R. *Single-Molecule Magnets and Related Phenomena*; Springer: Heidelberg, Germany, 2006; Vol. *122*. (c) Bartolomé, J.; Luis, F.; Fernandez, J. F. *Molecular Magnets*; Springer: Heidelberg, Germany, 2014. (d) Benelli, C.; Gatteschi, D. *Introduction to Molecular Magnetism. From Transition Metals to Lanthanides*; Wiley-VCH: Weinheim, Germany, 2015.

(2) (a) Woodruff, D. N.; Winpenny, R. E. P.; Layfield, R. *Chem. Rev.* **2013**, *113*, 5110−5148. (b) Sorace, L.; Benelli, C.; Gatteschi, D. *Chem. Soc. Rev.* **2011**, *40*, 3092−3104. (c) Luzon, J.; Sessoli, R. *Dalton Trans.* **2012**, *41*, 13556−13567. (d) Dreiser, J. *J. Phys.: Condens. Matter* **2015**, *27*, 183203.

(3) (a) Leuenberger, M. N.; Loss, D. *Nature* **2001**, *410*, 789−793. (b) Urdampilleta, M.; Klyatskaya, S.; Cleuziou, J.-P.; Ruben, M.; Wernsdorfer, W. *Nat. Mater.* **2011**, *10*, 502−506. (c) Vincent, R.; Klyatskaya, S.; Ruben, M.; Wernsdorfer, W.; Balestro, F. *Nature* **2012**, *488*, 357−360. (d) Ganzhorn, M.; Klyatskaya, S.; Ruben, M.; Wernsdorfer, W. *Nat. Nanotechnol.* **2013**, *8*, 165−169. (e) Thiele, S.; Balestro, F.; Ballou, R.; Klyatskaya, S.; Ruben, M.; Wernsdorfer, W. *Science* **2014**, *344*, 1135−1138.

(4) (a) Rinehart, J. D.; Fang, M.; Evans, W. J.; Long, J. R. *J. Am. Chem. Soc.* **2011**, *133*, 14236−14239. (b) Rinehart, J. D.; Fang, M.; Evans, W. J.; Long, J. R. *Nat. Chem.* **2011**, *3*, 538−542.

(5) Blagg, R. J.; Ungur, L.; Tuna, F.; Speak, J.; Comar, P.; Collison, D.; Wernsdorfer, W.; McInnes, E. J. L.; Chibotaru, L. F.; Winpenny, R. E. P. *Nat. Chem.* **2013**, *5*, 673−678.

(6) (a) Ishikawa, N.; Sugita, M.; Ishikawa, T.; Koshihara, S.; Kaizu, Y. *J. Am. Chem. Soc.* **2003**, *125*, 8694−8695. (b) Jiang, S.-D.; Wang, B.-W.; Su, G.; Wang, Z.-M.; Gao, S. *Angew. Chem., Int. Ed.* **2010**, *49*,

7448−7451. (c) Jiang, S.-D.; Wang, B.-W.; Sun, H.-L.; Wang, Z.-M.; Gao, S. *J. Am. Chem. Soc.* **2011**, *133*, 4730−4733. (d) Ganivet, C. R.; Ballesteros, B.; de la Torre, G.; Clemente-Juan, J. M.; Coronado, E.; Torres, T. *Chem. - Eur. J.* **2013**, *19*, 1457−1465. (e) Meihaus, K. R.; Long, J. R. *J. Am. Chem. Soc.* **2013**, *135*, 17952−17957. (f) Liu, J.-L.; Chen, Y.-C.; Zheng, Y.-Z.; Lin, W.-Q.; Ungur, L.; Wernsdorfer, W.; Chibotaru, L. F.; Tong, M. L. *Chem. Sci.* **2013**, *4*, 3310−3316. (g) Demir, S.; Zadrozny, J. M.; Long, J. R. *Chem. - Eur. J.* **2014**, *20*, 9524−9529. (h) Le Roy, J. J.; Korobkov, I.; Murugesu, M. *Chem. Commun.* **2014**, *50*, 1602−1604. (i) Zheng, P.; Zhang, L.; Wang, C.; Xue, S.; Lin, S.-Y.; Tang, J. *J. Am. Chem. Soc.* **2014**, *136*, 4484−4487. (j) Brown, A. J.; Pinkowicz, D.; Saber, M. R.; Dunbar, K. R. *Angew. Chem., Int. Ed.* **2015**, *54*, 5864−5868.

(7) (a) Luzon, J.; Sessoli, R. *Dalton Trans.* **2012**, *41*, 13556−13567. (b) Chibotaru, L. F. *Struct. Bonding (Berlin)* **2015**, *164*, 185−230. (c) Chilton, N. F. *Inorg. Chem.* **2015**, *54*, 2097−2099. (d) Ungur, L.; Chibotaru, L. F. Computational Modelling of the Magnetic Properties of Lanthanide Compounds. In *Lanthanides and Actinides in Molecular Magnetism*; Layfield, R. A., and Murugesu, M., Eds.; Wiley-VCH Verlag GmbH & Co. KGaA: Weinheim, Germany, 2015; DOI: 10.1002/9783527673476.ch5.

(8) Pedersen, K. S.; Woodruff, D. N.; Bendix, J.; Clérac, R. Experimental Aspects of Lanthanide Single-Molecule Magnet Physics. In *Lanthanides and Actinides in Molecular Magnetism*; Layfield, R. A., and Murugesu, M., Eds.; Wiley-VCH Verlag GmbH & Co. KGaA: Weinheim, Germany, 2015; DOI: 10.1002/9783527673476.ch5.

(9) Orbach, R. *Proc. R. Soc. London, Ser. A* **1961**, *264*, 458−484.

(10) Guo, Y.-N.; Xu, G.-F.; Guo, Y.; Tang, J.-K. *Dalton Trans.* **2011**, *40*, 9953−9963.

(11) Finn, C. B. P.; Orbach, R.; Wolf, W. P. *Proc. Phys. Soc., London* **1961**, *77*, 261−268.

(12) Pedersen, K. S.; Ungur, L.; Sigrist, M.; Sundt, A.; Schau-Magnussen, M.; Vieru, V.; Mutka, H.; Rols, S.; Weihe, H.; Waldmann, O.; Chibotaru, L. F.; Bendix, J.; Dreiser, J. *Chem. Sci.* **2014**, *5*, 1650−1660.

(13) Marx, R.; Moro, F.; Dörfel, M.; Ungur, L.; Waters, M.; Jiang, S. D.; Orlita, M.; Taylor, M. J.; Frey, W.; Chibotaru, L. F.; van Slageren, J. *Chem. Sci.* **2014**, *5*, 3287−3293.

(14) (a) Cucinotta, G.; Perfetti, M.; Luzon, J.; Etienne, M.; Car, P.-E.; Caneschi, A.; Calvez, G.; Bernot, K.; Sessoli, R. *Angew. Chem., Int. Ed.* **2012**, *51*, 1606−1610. (b) Long, J.; Rouquette, J.; Thibaud, J.-M.; Ferreira, R. A. S.; Carlos, L. D.; Donnadieu, B.; Vieru, V.; Chibotaru, L. F.; Konczewicz, L.; Haines, J.; Guari, Y.; Larionova, J. *Angew. Chem., Int. Ed.* **2015**, *54*, 2236−2240.

(15) The Orbach mechanism has been expected to be dominant only in cases in which $k_B\Theta_D$, Θ_D being the Debye temperature, exceeds the energy of the excited ligand field state (cf. ref 9).

(16) Thomas, L.; Lionti, F.; Ballou, R.; Gatteschi, D.; Sessoli, R.; Barbara, B. *Nature* **1996**, *383*, 145−147.

(17) Bernhardt, P. V.; Flanagan, B. M.; Riley, M. *Aust. J. Chem.* **2000**, *53*, 229−231.

(18) Flanagan, B. M.; Bernhardt, P. V.; Krausz, E. R.; Lüthi, S. R.; Riley, M. J. *Inorg. Chem.* **2002**, *41*, 5024−5033.

(19) Lucaccini, E.; Sorace, L.; Perfetti, M.; Costes, J.-P.; Sessoli, R. *Chem. Commun.* **2014**, *50*, 1648−1651.

(20) Perfetti, M.; Lucaccini, E.; Sorace, L.; Costes, J. P.; Sessoli, R. *Inorg. Chem.* **2015**, *54*, 3090−3092.

(21) Dreiser, J.; Wäckerlin, C.; Ali, Md. E.; Piamonteze, C.; Donati, F.; Singha, A.; Pedersen, K. S.; Rusponi, S.; Bendix, J.; Oppeneer, P. M.; Jung, T. M.; Brune, H. *ACS Nano* **2014**, *8*, 4662−4671.

(22) Buchanan, R. A.; Wickersheim, K. A.; Pearson, J. J.; Herrmann, G. F. *Phys. Rev.* **1967**, *159*, 245−251.

(23) Reinhard, C.; Güdel, H.-U. *Inorg. Chem.* **2002**, *41*, 1048−1055.

(24) Urland, W.; Kremer, R.; Furrer, A. *Chem. Phys. Lett.* **1986**, *132*, 113−115.

(25) (a) Gómez-Coca, S.; Urtizberea, A.; Cremades, E.; Alonso, P. J.; Camón, A.; Ruiz, E.; Luis, F. *Nat. Commun.* **2014**, *5*, 4300. (b) Pedersen, K. S.; Sigrist, M.; Sørensen, M. A.; Barra, A.-L.; Weyhermüller, T.; Piligkos, S.; Thuesen, C.; Aa; Vinum, M. G.; Mutka, H.; Weihe, H.; Clérac, R.; Bendix, J. *Angew. Chem., Int. Ed.* **2014**, *53*, 1351−1354.

(26) Burzurí, E.; Carbonera, Ch.; Luis, F.; Ruiz-Molina, D.; Lampropoulos, C.; Christou, G. *Phys. Rev. B: Condens. Matter Mater. Phys.* **2009**, *80*, 224428.

(27) As the definition of SMMs given in the introduction does not rely on the presence or absence of external fields, the term is in line with literature practice applicable to **1**.

(28) Cole, K. S.; Cole, R. H. *J. Chem. Phys.* **1941**, *9*, 341−352.

(29) Soeteman, J.; Bevaart, L.; van Duyneveldt, A. J. *Physica* **1974**, *74*, 126−134.

(30) Zadrozny, J. M.; Atanasov, M.; Bryan, A. M.; Lin, C.-Y.; Rekken, B. D.; Power, P. P.; Neese, F.; Long, J. R. *Chem. Sci.* **2013**, *4*, 125−138.

(31) In the case that one would assume that our assignment of the nature of the observed transitions is erroneous, the smallest possible energy difference between the ground and excited doublets of $^2F_{7/2}$ would be ~170 cm^{-1}, corresponding to band v2 or v2′ (Figure 4). The simulated behavior for Δ_{Orbach} = 170 cm^{-1} is shown in Figure 6b as a solid blue line.

(32) Flanagan, B. M.; Bernhardt, P. V.; Krausz, E. R.; Lüthi, S. R.; Riley, M. J. *Inorg. Chem.* **2001**, *40*, 5401−5407.

(33) Abragam, A.; Bleaney, B. *Electron Paramagnetic Resonances of Transition Ions*; Oxford University Press: Oxford, U.K., 1970.

(34) Scott, P. L.; Jeffries, C. D. *Phys. Rev.* **1962**, *127*, 32−51.

(35) (a) van Vleck, J. H. *Phys. Rev.* **1940**, *57*, 426−447. (b) van den Broek, J.; van der Marel, L. C. *Physica* **1963**, *29*, 948−964.

(36) Orbach, R. *Proc. R. Soc. London, Ser. A* **1961**, *264*, 485−495.

(37) (a) Novak, M. A.; Sessoli, R.; Caneschi, A.; Gatteschi, D. *J. Magn. Magn. Mater.* **1995**, *146*, 211−213. (b) Gomes, A. M.; Novak, M. A.; Sessoli, R.; Caneschi, A.; Gatteschi, D. *Phys. Rev. B: Condens. Matter Mater. Phys.* **1998**, *57*, 5021−5024. (c) Fominaya, F.; Villain, J.; Fournier, T.; Gandit, P.; Chaussy, J.; Fort, A.; Caneschi, A. *Phys. Rev. B: Condens. Matter Mater. Phys.* **1999**, *59*, 519−528. (d) Evangelisti, M.; Luis, F.; Mettes, F. L.; Sessoli, R.; de Jongh, L. J. *Phys. Rev. Lett.* **2005**, *95*, 227206.